

Hyperon single-particle potentials in nuclear matter based on baryon-baryon interactions derived within chiral effective field theory

Asanosuke JINNO¹, Johann HAIDENBAUER², and Ulf-G. MEIßNER^{3,2}

¹*Department of Physics, Faculty of Science, Kyoto University, 606-8502, Japan,*

²*Institute for Advanced Simulation (IAS-4), Forschungszentrum Jülich, D-52425 Jülich, Germany,*

³*Helmholtz-Institut für Strahlen- und Kernphysik and Bethe Center for Theoretical Physics, Universität Bonn, D-53115 Bonn, Germany*

E-mail: jinno.asanosuke.36w@st.kyoto-u.ac.jp

(Received December 22, 2025)

An analysis of the Λ and Σ single-particle potentials is presented, based on YN interactions derived within chiral effective field theory up to next-to-next-to-leading order ($N^2\text{LO}$). The self-consistent Brueckner-Hartree-Fock framework is employed within the continuous choice for the single-particle potential. The result for the Λ single-particle potential is comparable to the ones obtained with previous chiral YN interactions up to next-to-leading order (NLO). The Σ single-particle potential is found weakly attractive, in contrast to earlier weakly repulsive results, reflecting new constraints from the recent J-PARC E40 data on Σ^+p scattering. An estimate of the theoretical uncertainty of the single-particle potentials is provided.

KEYWORDS: YN interaction, hyperons in nuclear matter

1. Introduction

The hyperon puzzle of neutron stars refers to the problem that most of the equations of state that include hyperons are not sufficiently stiff to support the observed massive neutron stars [1]. Although fifteen years have passed since the first report of such neutron stars, it is still controversial what mechanisms could prevent hyperons from appearing in neutron stars, not least due to insufficient constraints on the interactions between hyperons and nuclear matter. A key ingredient for discussing the appearance of hyperons in neutron stars is the corresponding single-particle potential in dense matter, in particular the one of the Λ hyperon.

In 2023, a hyperon-nucleon (YN) potential based on chiral effective field theory (χEFT) up to next-to-next-to-leading order ($N^2\text{LO}$) was presented [2], as an extension of previous works up to next-to-leading order (NLO) [3, 4]. The new interaction builds on a novel regularization scheme, the so-called semi-local momentum space (SMS) regularization, which has been shown to work rather well in the nucleon-nucleon (NN) sector [5]. Furthermore, the potential incorporates new constraints on the Σ^+p and Σ^-p differential cross sections from recent J-PARC E40 experiments [6].

In this contribution, we present selected results from an extended analysis of the Λ and Σ single-particle potentials U_Λ and U_Σ [7], for the SMS YN interaction up to $N^2\text{LO}$ in combination with NN forces likewise derived in the SMS scheme [5]. The self-consistent Brueckner-Hartree-Fock method is employed [8], within the continuous choice for the single-particle potential, and results for the density dependence of U_Λ and U_Σ are reported. An

Table I. Partial-wave contributions to $U_\Lambda(k = 0)$ (in MeV) at $k_F = 1.35 \text{ fm}^{-1}$. Results are presented for the SMS YN interactions at different chiral orders and with different cutoffs [2] and, in addition, for the NLO13(500) [3] and NLO19(500) [4] interactions.

	1S_0	$^3S_1 + ^3D_1$	3P_0	1P_1	3P_1	$^3P_2 + ^3F_2$	Total
SMS LO(700)	-13.9	-28.2	-1.0	0.7	1.0	-0.8	-42.4
SMS NLO(500)	-15.7	-25.6	0.4	4.5	2.0	-3.2	-37.7
SMS NLO(550)	-15.0	-24.5	0.5	2.5	1.5	-4.1	-39.3
SMS NLO(600)	-12.5	-20.2	0.4	1.0	1.5	-4.0	-34.0
SMS N ² LO(500)	-16.2	-24.8	0.3	2.9	0.6	-3.2	-41.2
SMS N ² LO(550) ^a	-15.2	-26.9	0.1	1.2	0.9	-4.9	-45.8
SMS N ² LO(550) ^b	-15.1	-27.3	0.4	1.5	1.6	-3.4	-43.4
SMS N ² LO(600)	-15.3	-25.4	0.2	1.6	1.0	-5.0	-44.1
NLO13(500)	-15.3	-18.9	0.9	0.2	1.6	-1.3	-33.1
NLO19(500)	-13.5	-28.7	0.9	0.3	1.6	-1.2	-40.9

estimate of the theoretical uncertainty of the single-particle potentials in symmetric nuclear matter (SNM) and in pure neutron matter (PNM) is provided.

2. Results

Results for the Λ single-particle potential U_Λ in SNM are presented in Table I and in Fig. 1. The notation for the employed YN interactions is adopted from Ref. [2] and specifies the various potentials by their chiral order and by the employed cutoff mass. The superscripts a and b in case of SMS N²LO(550) refer to variants with different P -wave interactions [2]. The required nucleon single-particle potential U_N is evaluated from the SMS N⁴LO⁺ NN force [5] with cutoff 450 MeV.

Table I summarizes the results for the Λ single-particle potential U_Λ and its partial-wave decomposition at nuclear matter saturation density ($\rho_0 = 2k_F^3/(3\pi^2)$, with the Fermi momentum $k_F = 1.35 \text{ fm}^{-1}$), and for zero momentum of Λ . In lowest order of the hole-line expansion, this quantity represents the binding energy of the Λ in infinite nuclear matter and can be compared with the quasi-empirical value inferred from hypernuclear experiments, which amounts to $U_\Lambda(\rho_0) \approx -30 \text{ MeV}$ [9]. The values of $U_\Lambda(k = 0)$ predicted by the SMS N²LO potentials range from -41 to -46 MeV, those of the NLO potentials are between -34 and -39 MeV [7]. The predictions for the YN potentials from 2019 (NLO19 [4]) and 2013 (NLO13 [3]), -41 MeV and -33 MeV, respectively, are comparable to the SMS results. A recent phenomenological analysis with a Λ -nucleus optical potential [10] suggests indeed that the YN two-body contribution to $U_\Lambda(\rho_0)$ is $-38.6 \pm 0.8 \text{ MeV}$ and attributes the difference of $11.3 \pm 1.4 \text{ MeV}$ to the quasi-empirical value to repulsive three-body forces. In this context, see also the Skyrme model calculation in Ref. [12] which includes likewise many-body effects.

In Fig. 1, the density dependence of U_Λ is presented. For the SMS interactions with a cutoff of 500 MeV, and also for NLO13 and NLO19, U_Λ reaches a minimum in the considered density range, whereas for the SMS NLO and N²LO interactions with larger cutoffs the minimum occurs at somewhat higher density. The case of NLO13 is special because there is already a pronounced trend towards a repulsive U_Λ from around $1.5\rho_0$ onwards, while a much slower variation with density is observed for the other interactions. As known from the work of Gerstung *et al.*, U_Λ for NLO13 eventually changes sign, i.e. becomes repulsive, around $2.5\rho_0$ [11]. The origin of the strikingly different behavior of the U_Λ results for NLO13

and NLO19 has been thoroughly discussed in Ref. [4]. It is a consequence of a marked difference in the strength of the ΛN - ΣN transition potential between the two sets of YN interactions. In essence, the larger (smaller) channel-coupling strength of NLO13 (NLO19) leads to less attractive (more attractive) U_Λ , even when the corresponding YN scattering results, including the ΛN - ΣN transition cross sections, are identical. As likewise discussed in Ref. [4], the strength of the ΛN - ΣN transition potential itself is not an observable and is closely connected with possible contributions from ΛNN three-body forces.

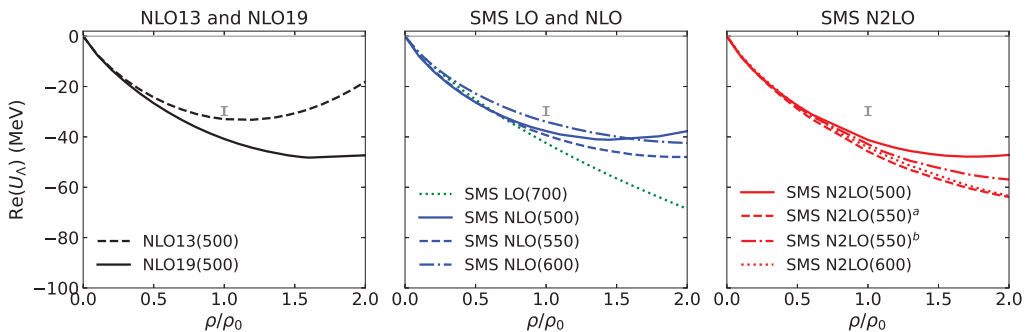


Fig. 1. Density dependence of the Λ single-particle potential in symmetric nuclear matter. The bar symbolizes the quasi-empirical value [9].

Table II. Partial-wave contributions to the real part of $U_\Sigma(k = 0)$ (in MeV) at $k_F = 1.35$ fm $^{-1}$. Same description of interactions as in Table I.

	Isospin $I = 1/2$			Isospin $I = 3/2$			Total
	1S_0	$^3S_1 + ^3D_1$	P	1S_0	$^3S_1 + ^3D_1$	P	
SMS LO(700)	7.1	-16.7	-1.9	-10.4	24.7	-1.5	1.0
SMS NLO(550)	8.0	-25.0	-0.3	-10.7	20.3	-3.4	-11.3
SMS N ² LO(550) ^a	7.5	-24.9	3.4	-11.0	20.0	-4.4	-10.3
SMS N ² LO(550) ^b	7.5	-24.8	3.6	-11.0	20.0	-5.0	-11.0
NLO13(500)	6.2	-26.2	3.7	-11.1	32.5	-0.8	3.7
NLO19(500)	6.0	-19.5	3.8	-10.4	32.7	-0.8	11.2

Total results and the partial-wave decomposition for the Σ single-particle potential at ρ_0 are listed in Table II. The range for U_Σ deduced from phenomenological analyses of data on Σ^- atoms and (π^-, K^+) spectra is 10–50 MeV [9]. Obviously, only the SMS LO interaction yields repulsive results, while the SMS NLO and N²LO potentials predict an attractive Σ potential. In contrast, NLO13 as well as NLO19 yield a repulsive U_Σ at ρ_0 . The primary reason for the difference is that the contribution from the 3S_1 - 3D_1 partial wave with isospin $I = 3/2$ is noticeably more repulsive for NLO13 and NLO19 than that of the SMS YN potentials, as can be seen from the isospin decomposition. A reduction of the interaction strength in that channel has become necessary due to constraints from recent J-PARC E40 data on $\Sigma^+ p$ scattering [6]. The YN potentials NLO13 and NLO19 overshoot those data, see Fig. 2. Specifically, they predict an unrealistic rise in the integrated cross section for large momenta (right side) caused by an artificial increase of repulsion in the 3S_1 partial wave (left side).

Figure 3 shows the density dependence of U_Σ . The SMS NLO and N²LO potentials predict an attractive U_Σ throughout, except for the potentials with a cutoff of 500 MeV where U_Σ turns to repulsion at around $1.5 \rho_0$. The results for NLO13 and NLO19 are radically different. Here, U_Σ becomes repulsive already at lower densities, and moreover the repulsion increases rapidly with density. As already discussed above, the different behavior is a consequence of the constraints by the J-PARC E40 $\Sigma^+ p$ data [6] on the ΣN interaction in the $I = 3/2$ channel that have been taken into account in the SMS YN potentials.

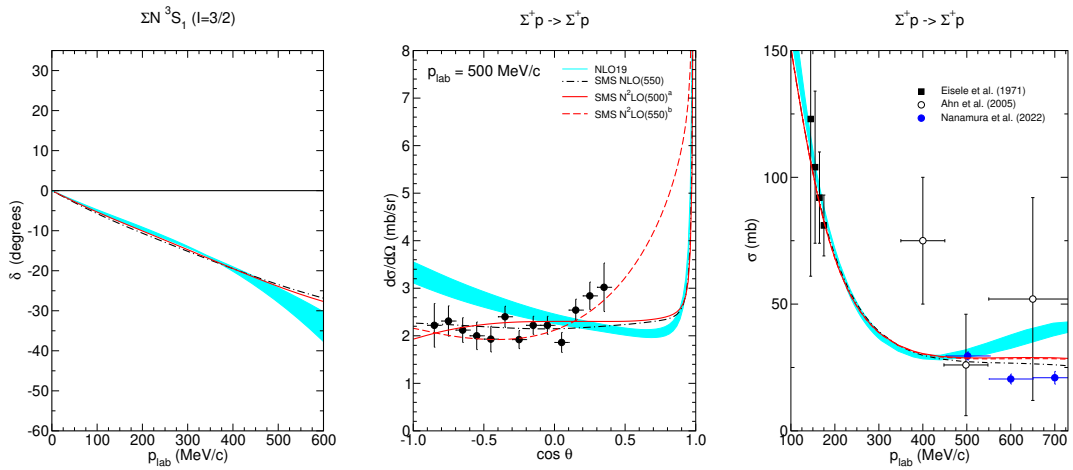


Fig. 2. $\Sigma^+ p$ scattering results [2]. Left: 3S_1 phase shift. Center: Differential cross section at 500 MeV/c. Right: Integrated $\Sigma^+ p$ cross section. Solid, dashed, and dash-dotted lines are the results for the SMS N²LO(550)^a, N²LO(550)^b, and NLO(550) potentials, respectively. The band represents the results of the NLO19 potential from Ref. [4]. The E40 data [6] are indicated by filled circles.

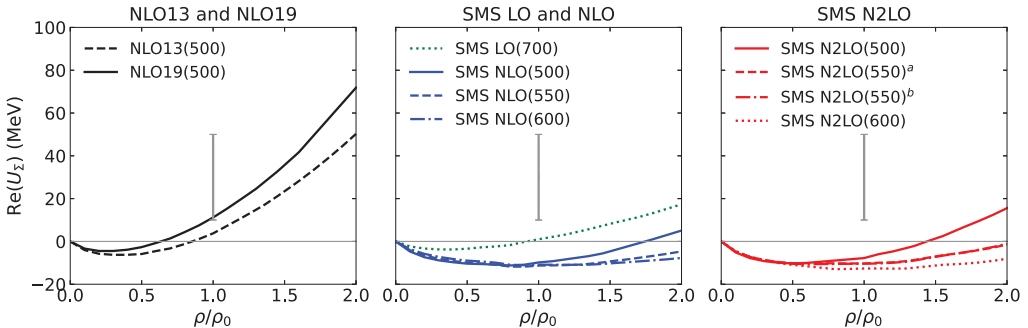


Fig. 3. Density dependence of the Σ single-particle potential in symmetric nuclear matter. The bar indicates results from phenomenological analyses [9].

3. Uncertainty estimate

χ EFT has not only the salient feature that there is an underlying power counting that allows to improve calculations systematically by going to higher orders in the perturbative expansion, it also allows to estimate the theoretical uncertainty due to the truncation in that expansion. Below, we discuss the truncation error for U_Λ and U_Σ , following the method

proposed by Epelbaum, Krebs, and Meißner (EKM) [13, 14]. It combines information about the expected size and the actual size of higher-order corrections. It can be applied to any observable X that has been evaluated up to a specific order i in the chiral expansion, $X^{(i)}$. The concrete expressions for the corresponding uncertainty $\delta X^{(i)}$ are [13],

$$\begin{aligned}\delta X^{\text{LO}} &= Q^2 |X^{\text{LO}}|, \quad \delta X^{\text{NLO}} = \max \left(Q^3 |X^{\text{LO}}|, Q |X^{\text{NLO}} - X^{\text{LO}}| \right), \\ \delta X^{\text{N}^2\text{LO}} &= \max \left(Q^4 |X^{\text{LO}}|, Q^2 |X^{\text{NLO}} - X^{\text{LO}}|, Q |X^{\text{N}^2\text{LO}} - X^{\text{NLO}}| \right),\end{aligned}\quad (1)$$

with the additional constraint for the theoretical uncertainties at LO and NLO to have at least the size of the actual higher-order contributions [13]. Here, Q represents the expansion scale in the chiral expansion, which is given by $Q \in \{p/\Lambda_b, M_\pi/\Lambda_b\}$, where p is the typical momentum of the baryons, M_π is the pion mass, and Λ_b is the breakdown scale of the chiral expansion. In a past application of this method to nuclear matter properties by Hu *et al.* [15], the momentum scale p has been identified with the Fermi momentum k_F . We adopt the same prescription in our work. For the breakdown scale, $\Lambda_b = 480$ and 600 MeV are used for SNM and PNM, respectively, a choice guided by the Bayesian analysis of nuclear matter properties by Hu *et al.* [16].

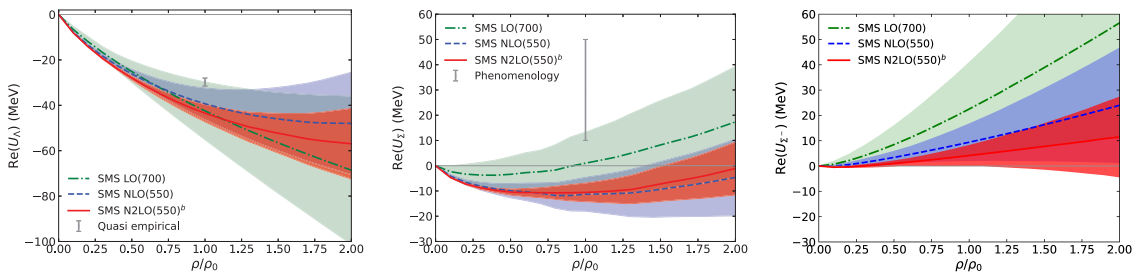


Fig. 4. Uncertainty estimate of the Λ and Σ single-particle potentials in symmetric nuclear matter and of the Σ^- single-particle potential in pure neutron matter, from left to right. The SMS NLO and N^2LO^b interactions with cutoff 550 MeV are employed, while for SMS LO the potential with 700 MeV cutoff is used. The bars symbolize the values from Ref. [9].

In Fig. 4, the uncertainty estimates for the density dependence of $U_\Lambda(k=0)$ and $U_\Sigma(k=0)$ are shown. The SMS LO(700), NLO(550), and $\text{N}^2\text{LO}(550)^b$ YN potentials have been selected as exemplary set. The other cutoffs of 500 and 600 MeV result in very similar uncertainty bands. As one can see, the uncertainty of the predicted single-particle potentials increases rapidly with density and is already substantial at the highest density considered.

Regarding the Λ single-particle potential at ρ_0 , the results for the LO and NLO interactions are more or less in line with the quasi-empirical value of $U_\Lambda(\rho_0) \approx -30$ MeV within the uncertainty estimate, see left side of Fig. 4. To be concrete, $U_\Lambda^{\text{NLO}}(\rho_0) = -39.3 \pm 7.0$ MeV. The uncertainty of the NLO result provides also a measure for the size of possible YNN three-body forces which start to contribute at N^2LO . Interestingly, the present estimate is compatible with the actual contribution of an effective three-body force evaluated in Ref. [11], established within the assumption of decuplet saturation and based on LECs constrained from dimensional scaling arguments. It is also comparable to the value suggested in Ref. [10] within a phenomenological analysis. The estimate for the N^2LO result at ρ_0 , $U_\Lambda^{\text{N}^2\text{LO}}(\rho_0) = -43.5 \pm 3.8$ MeV, is not compatible with the quasi-empirical value. Note, however, that the calculation at N^2LO is incomplete, i.e. three-body forces are missing! Thus, as a matter of fact, the actual uncertainty is here still the one obtained for the result at NLO.

The uncertainty estimate for Σ in SNM is shown in the center of Fig. 4. The result at ρ_0 is $U_{\Sigma}^{\text{NLO}}(\rho_0) = -11.3 \pm 6.7$ MeV and $U_{\Sigma}^{\text{N}^2\text{LO}}(\rho_0) = -10.6 \pm 3.7$ MeV. The uncertainty bands for the NLO and N^2LO potentials are similar because there is not much difference between the results at NLO and N^2LO , as can be seen from Fig. 3. Obviously, U_{Σ} is predicted to be attractive up to $1.5 \rho_0$, even when considering the theoretical uncertainty. At the right side of Fig. 4, the uncertainty estimate for the Σ^- single-particle potential in PNM is shown. The values at ρ_0 are $U_{\Sigma^-}^{\text{NLO}}(\rho_0) = 9.4 \pm 7.2$ MeV and $U_{\Sigma^-}^{\text{N}^2\text{LO}}(\rho_0) = 4.1 \pm 4.0$ MeV. Compared to the case of U_{Σ} in SNM, the N^2LO uncertainty band is noticeably larger due to the fact that for a given ρ_0 the Fermi momentum in PNM is larger. Obviously U_{Σ^-} is predominantly repulsive, for the NLO as well as for the N^2LO potential.

4. Summary and Outlook

In this contribution, we reported results for the in-medium properties of the hyperons Λ and Σ , based on a recent YN interaction up to N^2LO in the chiral expansion, established by the Jülich-Bonn group [2]. It turned out that the Λ single-particle potentials predicted by the new NLO and N^2LO potentials are slightly more attractive at nuclear matter saturation density than the quasi-empirical value. The Σ single-particle potentials are found weakly attractive at the saturation density.

Next, YNN three-body forces have to be included in order to complete the calculation up to N^2LO . Their explicit computation is, unfortunately, rather challenging since, in principle, one needs to solve the Bethe-Faddeev equations. However, as alternative and simplification one can consider an approximate treatment by summing one of the nucleons over the occupied states in the Fermi sea which then leads to an effective density-dependent two-body interaction [17,18]. Of course, for being more consistent with available hypernuclear few-body calculations [19,20] the so far adopted on-shell approximation [11,21] should be avoided.

References

- [1] G. F. Burgio, H. J. Schulze, I. Vidaña and J. B. Wei, *Prog. Part. Nucl. Phys.* **120**, 103879 (2021).
- [2] J. Haidenbauer, U.-G. Meißner, A. Nogga and H. Le, *Eur. Phys. J. A* **59**, 63 (2023).
- [3] J. Haidenbauer *et al.*, *Nucl. Phys. A* **915**, 24 (2013).
- [4] J. Haidenbauer, U.-G. Meißner and A. Nogga, *Eur. Phys. J. A* **56**, 91 (2020).
- [5] P. Reinert, H. Krebs and E. Epelbaum, *Eur. Phys. J. A* **54**, 86 (2018).
- [6] T. Nanamura *et al.* [J-PARC E40], *PTEP* **2022**, 093D01 (2022).
- [7] A. Jinno, J. Haidenbauer and U.-G. Meißner, *Phys. Rev. C* **112**, 065209 (2025).
- [8] S. Petschauer *et al.*, *Eur. Phys. J. A* **52**, 15 (2016).
- [9] A. Gal, E. V. Hungerford and D. J. Millener, *Rev. Mod. Phys.* **88**, 035004 (2016).
- [10] E. Friedman and A. Gal, *Nucl. Phys. A* **1039**, 122725 (2023).
- [11] D. Gerstung, N. Kaiser and W. Weise, *Eur. Phys. J. A* **56**, 175 (2020).
- [12] A. Jinno, K. Murase, Y. Nara and A. Ohnishi, *Phys. Rev. C* **108**, 065803 (2023).
- [13] E. Epelbaum, H. Krebs and U.-G. Meißner, *Eur. Phys. J. A* **51**, 53 (2015).
- [14] S. Binder *et al.* [LENPIC], *Phys. Rev. C* **93**, 044002 (2016).
- [15] J. Hu, Y. Zhang, E. Epelbaum, U.-G. Meißner and J. Meng, *Phys. Rev. C* **96**, 034307 (2017).
- [16] J. Hu, P. Wei and Y. Zhang, *Phys. Lett. B* **798**, 134982 (2019).
- [17] J. W. Holt, M. Kawaguchi and N. Kaiser, *Front. in Phys.* **8**, 100 (2020).
- [18] S. Petschauer *et al.*, *Nucl. Phys. A* **957**, 347 (2017).
- [19] H. Le, J. Haidenbauer, U.-G. Meißner and A. Nogga, *Eur. Phys. J. A* **60**, 3 (2024).
- [20] H. Le, J. Haidenbauer, U.-G. Meißner and A. Nogga, *Phys. Rev. Lett.* **134**, 072502 (2025).
- [21] J. Haidenbauer, U.-G. Meißner, N. Kaiser and W. Weise, *Eur. Phys. J. A* **53**, 121 (2017).